

The Joint Use of Multi-Platform Satellite InSAR Data and Geotechnical Models for the Study of the Shanghai Ocean-Reclaimed Lands

Antonio Pepe ^{1,*}, Manuela Bonano ¹, Qing Zhao ^{2,3}, Tianliang Yang ^{4,5}, Hanmei Wang ^{4,5}

¹ Institute for Electromagnetic Sensing of the Environment, Italian National Research Council, via Diocleziano 328, 80124 Napoli, Italy; E-Mails: pepe.a@irea.cnr.it (A. P.); bonano.m@irea.cnr.it (M. B.).

² Key Laboratory of Geographical Information Science, Ministry of Education, East China Normal University, Shanghai 200062, China.

³ Joint Laboratory for Environmental Remote Sensing and Data Assimilation, East China Normal University, Shanghai 200062, China; E-mail: qzhao@geo.ecnu.edu.cn (Q. Z.).

⁴ Shanghai Surveying and Mapping Institute, Shanghai 200072, China.

⁵ Key Laboratory of Land Subsidence Monitoring and Prevention, Ministry of Land and Resources, Shanghai 200072, China; E-mails: sigs_ytl@163.com (T. Y.); hanmeiw@163.com (H. W.).

* Author to whom correspondence should be addressed; E-Mail: pepe.a@irea.cnr.it; Tel.: +39-081762617.

Abstract: We present in this work the results of a multi-platform Differential Interferometry Synthetic Aperture Radar (DInSAR) analysis, which is aimed at investigating the surface displacements occurred over the past few years in the ocean-reclaimed platforms of the Shanghai megacity (China). To this purpose, the advanced multi-temporal Small Baseline Subset (SBAS) algorithm has been applied to two sequences of SAR images collected by the ASAR/ENVISAT and by the COSMO-SkyMed (CSK) sensors, respectively, from the year 2007 to 2016. The long time gap (of about three years) existing between the available ASAR/ENVISAT and CSK datasets has given rise to additional difficulties for their joint exploitation and combination. This problem has successfully been solved by benefiting from the knowledge of a time-dependent model that describes the temporal evolution of the expected deformations affecting the Shanghai ocean-reclaimed platforms. As a result, we have retrieved surface displacement time-series that are helpful for a better understanding of the on-going deformation phenomena. As an outcome, we have found that ocean-reclaimed platforms have been experienced from 2007 to 2016 an average cumulative ground displacement of about 25 cm.

Keywords: deformation; interferometry; geotechnical models; non-linear problem; synthetic aperture radar (SAR); time-series

1. Introduction

A feasible measure to solve the problem of land scarcity in lowland countries and coastal cities is to make land from reclamation of the sea. The Netherlands, for instance, has reclaimed land since the sixteenth century and up to now, one-third of its territory lies at heights lower than the mean sea level [1]. The Changi Airport in Singapore, the Honk Hong international Airport in China, the Kansai airport in Japan and the New Doha International Airport in Qatar are all built on reclaimed and/or partially reclaimed lands [2-7]. Ocean-reclaimed platforms are, however, seriously affected by settlements that may cause severe damages to buildings, highways, airport runways, harbors, and underground facilities, thus also resulting in a possible decrease of the sea walls height. In China, 1600 Km² of land was reclaimed from 2002 to 2011 [8-11]. One of the most important reclamation projects is the one relevant to Lingang New City (new name Nanhui New City) of Shanghai (see Figure 1) under which about 130 Km² of land was reclaimed from the sea from 2003 to 2006; this project also plans to make 1000 Km² of new lands from the Yangtze River mount by the year 2020 [10].

The ocean-reclaimed area, which extends for about 300 km² (45% of which reclaimed from intertidal wetlands) has been subject over recent years to broad modifications in its geo-morphology and urban environment. Indeed, two main inherent problems arise for land-reclaimed areas: liquefaction and ground settlement and both of them may cause serious ground failures and damages to infrastructures on reclaimed foundations [12-14]. Moreover, the results of geotechnical analyses have revealed that such a kind of settlement continues over the entire reclamation facility lifetime. Temporal evolution of settlements can be distinguished in a primary consolidation phase of alluvial deposits phase, in a long-term creep (secondary compression stage) of the alluvial deposits beneath the reclamation, and finally in a creep within the reclamation fill [14]. These settlements may occur during and after reclamation foundation construction and, when not correctly predicted, can cause delays and considerable increases of the entire reclamation cost projects. Ground settlements of coastal reclaimed areas in Shanghai, which is caused by over pumping groundwater and consolidation of large-areas dredger fill and alluvial deposits, have already been observed and reported in the literature [15]-[20]. In particular, field measurements indicate that ground settlement of the reclaimed foundations occurred during the construction of the Lingang New City of Shanghai, with average cumulative values of deformation between 25 and 75 mm in six years (from 2001 to 2006), corresponding to average annual rates ranging between 5 and 15 mm/year [16]. Laboratory tests based on the principles of the consolidation theory [21] performed taking into account dredger fill type (alluvial deposits thickness, soil composition, water content) and other engineering parameters predicted that such residual settlements will also continue over the next years but with decreasing annual rates.

In this framework, the well-established remote sensing technique known to as Differential Synthetic Aperture Radar (SAR) Interferometry (DInSAR) [22]-[25] can play a strategic role for the detection and monitoring of the on-going surface deformation signals at a large spatial scale. Over the recent fifteen years, several advanced multi-temporal DInSAR techniques, aimed at investigating the time evolution of ground displacements, have been proposed [26]-[30]. Two families of multi-temporal DInSAR methods today broadly exist: the Persistent Scatterers (PS) [26-27] and the Small Baseline (SB) techniques [28-30]. The PS methods focus on the analysis of point-wise targets that are not seriously affected by decorrelation, and are particularly suitable for the monitoring of buildings and man-made objects in urban areas. Conversely, the SB approaches allow the investigation of displacement signals that affect distributed targets on the ground, making it possible to increase the spatial density of DInSAR measurements in semi-urbanized and/or rural areas. A popular method belonging to the class of the SB techniques is the Small Baseline Subset (SBAS) [28] approach. It relies on the least-squares (LS) inversion of a properly selected sequence of small baseline (SB) interferograms through the singular value decomposition (SVD) method [31]. Despite their inherent differences, both the PS and SB methods have been applied to monitor deformation phenomena due to several natural and anthropogenic hazards, such as volcanic events [32-33], earthquakes [34-36], landslides [37-38], tunneling excavations [39-40], terrain consolidation and land-subsidence of river deltas [41-43].

In this work, we investigate the complex deformation phenomena that have affected the coastal area of the Shanghai megacity. Our study is based on the application of the SBAS-DInSAR technique to two sets of SAR images collected at C-band by the ASAR/ENVISAT sensor, and at X-band by the COSMO-SkyMed (CSK) SAR constellation sensors. The processed SAR data span the whole time period between February 26, 2007 and March 18, 2016. However, due to the lack of a systematic acquisition plan of SAR data over the investigated area, there is a significant temporal gap (of about three years) between the available ENVISAT and CSK data frames. In fact, over the past few years, radar sensors mounted on board to satellite platforms have not regularly imaged the southern sector of the Shanghai coastal area. As a consequence, the present-day archives of SAR images are characterized by a reduced number of scenes with compatible acquisition geometries, and most of them only cover spotted areas of the whole region; in addition, a few time gaps among the different sets of the currently available SAR data sets are present. In order to overcome such key limitations and retrieve a unique displacement time-series from 2007 to present-days, via the combination of the

available CSK and ENVISAT datasets, we have developed and applied a dedicated strategy. Such method relies on the key assumption that over the areas under reclamation the observed deformations are mostly vertical, and it exploits the knowledge of proper geotechnical models [15,19,44-47] that are useful to predict the evolution of ground deformations mostly due to soil compaction mechanisms. The achieved results are in general agreement with previous studies [47-48] that reported Lingang New City was affected from 2007 to 2010 by annual subsidence rates between 12 and 18 mm/year, where higher rates were registered in the regions more proximal to the coast in correspondence to which reclamation projects started earlier.

The exploitation of multiple sets of SAR acquisitions collected at distinctive frequency bands as well as the knowledge of a time-dependent model for the expected subsidence in ocean-reclaimed platforms turns out helpful for the retrieval of displacement time-series over the whole 2007-2016 time-frame, thus allowing us to get up-to-date insights into the present and future evolution of the reclamation area settlements.

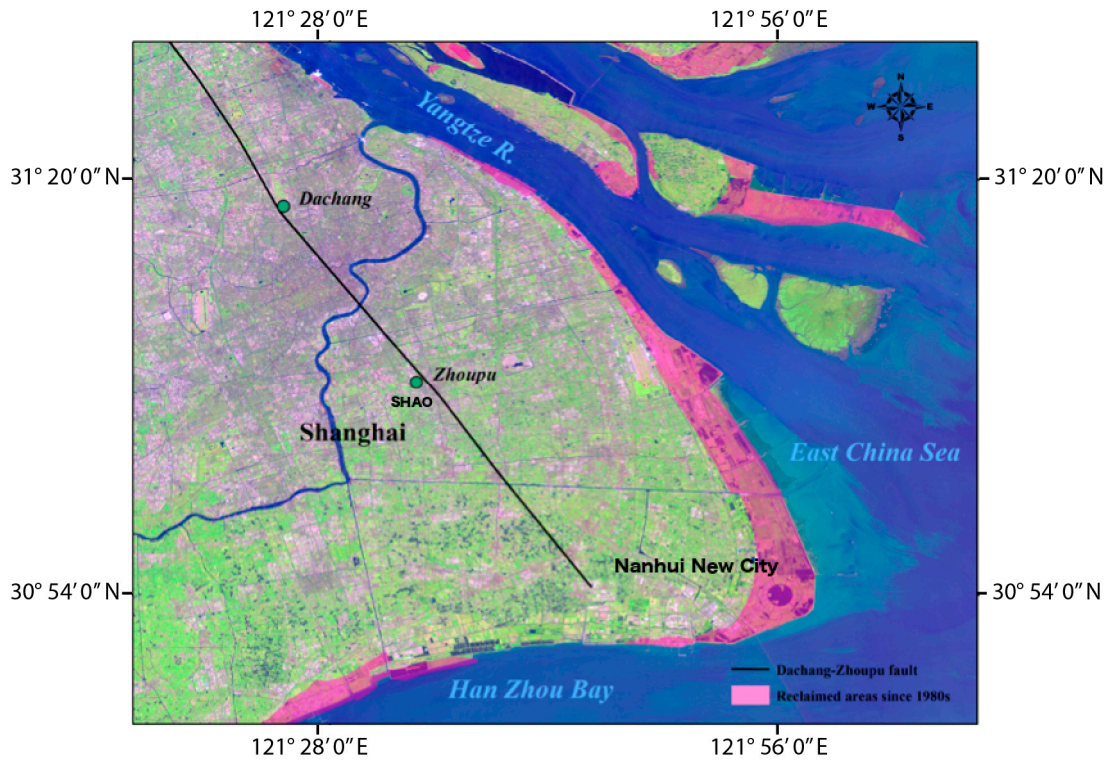


Figure 1. Landsat8 image collected on August 3, 2015, which shows the city of Shanghai and its coastal reclaimed areas (since 1980s) in Nanhui New City. Ocean-reclaimed areas are represented in pink, whereas the black line identifies the trace on the ground of the Dachang-Zhoupu fault.

2. Study Area

The megacity of Shanghai is located at the midpoint of the north-south coastline of China on the alluvial plain of the Yangtze River delta. Shanghai is bounded at north by the Yangtze River estuary, at east by the East China, and at south by the Hangzhou Bay. The deposits in the most part of the city are soft sediments that were formed during the Quaternary Era [49]. The buried depth of bed rocks ranges between 200 and 300 m. The land area of Shanghai extends for about 6000 km² and is at most flat, with altitude ranging between 2 and 6 m. It is crossed by the Yangtze River, which is the longest river in Asia and it is also ranked 4th globally in terms of sediment loads (470 Mt/year) [49]. The large amount of riverine sediment supply and the high total riverine sediment discharge rate in Yangtze River have made it possible for Shanghai to reclaim land along its eastern coastal areas. As matter of fact, Shanghai has continuously reclaimed coastal intertidal and wetland areas from the 1950s to build up new cities, ports, resorts, and industrial zones. New dykes have been built for trapping

sediments from Yangtze River and the coast, thus to make new lands, as evidenced in the recent Landsat8 images (see Figure 1). For ocean-land reclamation, dredging and hydraulic filling methods have been used. The dredger fill, which is a kind of unconsolidated soil with high water content, large void ratio and high compressibility, is blown-filled with the sludge and dredged out from the coastal seabed [50]. In particular, the reclamation procedure of Lingang New City (see Figure 1) started in 1994 and was almost completed in 2006 [51]. According to the engineering geology characteristics of the area, hydraulic fill soil is typically composed of two types of alluvial deposits [52]: Type A alluvial deposits were used in the western sector of the city, whereas Type B deposits were used in the newly reclaimed areas in the eastern part of the city, just in the near proximity of the coast. Previous analyses have already shown that Type A deposits are nowadays almost consolidated, being the observed surface deformation rates on the order of a few millimeters per year [15,19]. On the other hand, Type B alluvial deposits, which characterize the eastern sector of the city (just nearby the ocean) are still today subject to significant residual settlements (with maximum deformation rates of about 2-3 cm per year), as confirmed and further supported by the results of our recent investigations that are presented and discussed in this work.

3. Data and Methods

Two independent sets of stripmap SAR images acquired at C- and X-band have been integrated to carry out a comprehensive analysis of the deformation phenomena occurring over the area of Lingang New City (Shanghai). The first dataset is composed of $N_1 = 35$ SAR images collected at times $\mathbf{t}^{(1)} \equiv [t_1^{(1)}, t_2^{(1)}, \dots, t_{N_1}^{(1)}]^T$ by the ASAR/ENVISAT sensor [53] from February 26, 2007 to September 13, 2010 (ascending passes, VV polarization, Track 497, Frame 616, swath IS2, and a sensor side-looking angle of about 23°). The second dataset consists of $N_2 = 61$ SAR scenes acquired at times $\mathbf{t}^{(2)} \equiv [t_1^{(2)}, t_2^{(2)}, \dots, t_{N_2}^{(2)}]^T$ by the SAR sensors onboard the COSMO-SkyMed (CSK) satellites constellation [54] from December 7, 2013 to March 18, 2016 (HH polarization, descending passes, and a sensor side-looking angle of about 29°). The available ASAR/ENVISAT and CSK SAR data are listed in Table 2 and 3, respectively, and they are also pictorially represented in the temporal/perpendicular baseline plane (see the diamonds shown in Figure 2a and 2b, respectively). The proposed combination technique requires the preliminary generation from each dataset of the inherent LOS displacement time-series. This task is achieved by independently applying to the available SAR datasets the SBAS-DInSAR technique [28]. Subsequently, the computed Line-of-Sight (LOS)-projected time-series are geocoded to a common spatial grid of points.

Henceforth, let $\mathbf{d}^{(j)}(P) \equiv [d_1^{(j)}, d_2^{(j)}, \dots, d_{N_j}^{(j)}]^T$ $j = 1, 2; \forall P \in S$ be the geocoded LOS displacement time-series, with S being the group of high-coherent pixels that are in common to the two SAR datasets. We specifically remark that each LOS displacement time-series is only known in relative to a generic time acquisition [28], which is usually selected as the time when the first SAR image of the dataset was acquired, thus $d_1^{(j)} \equiv 0; j = 1, 2$. At this stage, we can observe that, for each common pixel of the geocoded grid, the relevant LOS deformation vectors $\mathbf{d}^{(j)}$ $j = 1, 2$ can generally be expressed in terms of the inherent 3-D components of the deformation [55-56], namely the East-West $\mathbf{E}^{(j)}$, $j = 1, 2; \forall P \in S$, the North-South $\mathbf{N}^{(j)}$, $j = 1, 2; \forall P \in S$ and the Up-Down (vertical) $\mathbf{h}^{(j)}(P)$ $j = 1, 2; \forall P \in S$ displacement vectors, as follows:

$$\mathbf{d}^{(j)}(P) = \sin \vartheta^{(j)} \cos \varphi^{(j)} \mathbf{E}^{(j)}(P) + \sin \vartheta^{(j)} \sin \varphi^{(j)} \mathbf{N}^{(j)}(P) + \cos \vartheta^{(j)} \mathbf{h}^{(j)}(P) \quad j = 1, 2; \forall P \in S \quad (1)$$

where $\vartheta^{(j)}$, $j = 1, 2$ are the side-looking angles of the ENVISAT and the CSK radar sensors, respectively, which are equal to $\vartheta^{(1)} \cong 23^\circ$ and $\vartheta^{(2)} \cong 29^\circ$, whereas $\varphi^{(1)} \cong 12^\circ$ and $\varphi^{(2)} \cong 8^\circ$ are the

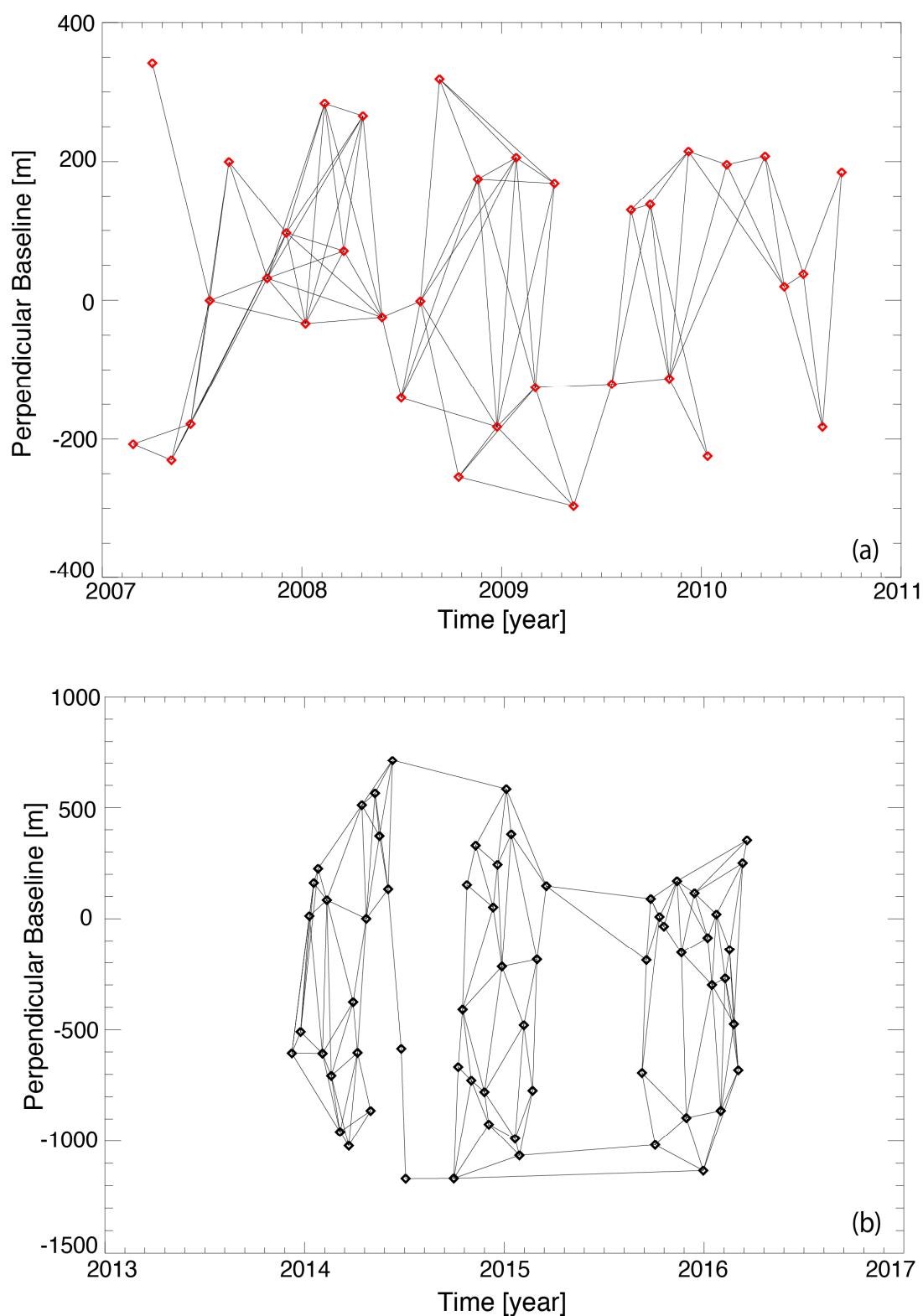


Figure 2. Distribution of the available ENVISAT/ASAR (a) and CSK (b) SAR data in the temporal/perpendicular baseline domain. SAR data are represented with red (a) and black (b) diamonds, whereas connecting arcs are representative of the selected SB interferometric data-pairs.

Table 1: ASAR/ENVISAT SAR Acquisition list

Mission	Day	Month	ear	Perpendicular Baseline [m]
ENVISAT	26	02	2007	-207
ENVISAT	02	04	2007	341
ENVISAT	07	05	2007	-230
ENVISAT	11	06	2007	-178
ENVISAT	16	07	2007	0
ENVISAT	20	08	2007	200
ENVISAT	29	10	2007	31
ENVISAT	03	12	2007	96
ENVISAT	07	01	2008	-33
ENVISAT	11	02	2008	283
ENVISAT	17	03	2008	70
ENVISAT	21	04	2008	266
ENVISAT	26	05	2008	-25
ENVISAT	30	06	2008	-141
ENVISAT	04	08	2008	-1
ENVISAT	08	09	2008	319
ENVISAT	13	10	2008	-254
ENVISAT	17	11	2008	174
ENVISAT	22	12	2008	-182
ENVISAT	26	01	2009	206
ENVISAT	02	03	2009	-126
ENVISAT	06	04	2009	169
ENVISAT	11	05	2009	-296
ENVISAT	20	07	2009	-120
ENVISAT	24	08	2009	130
ENVISAT	28	09	2009	137
ENVISAT	02	11	2009	-113
ENVISAT	07	12	2009	215
ENVISAT	11	01	2010	-225
ENVISAT	15	02	2010	196
ENVISAT	26	04	2010	208
ENVISAT	31	05	2010	20
ENVISAT	05	07	2010	38
ENVISAT	09	08	2010	-182
ENVISAT	13	09	2010	185

Table 2: CSK SAR Acquisition list

Mission	Day	Month	Year	Perpendicular Baseline [m]
CSK	07	12	2013	-606
CSK	23	12	2013	-509
CSK	08	01	2014	13
CSK	16	01	2014	161
CSK	24	01	2014	225
CSK	01	02	2014	-607
CSK	09	02	2014	84
CSK	17	02	2014	-707
CSK	05	03	2014	-958
CSK	21	03	2014	-1021
CSK	29	03	2014	-377
CSK	06	04	2014	-603
CSK	14	04	2014	511
CSK	22	04	2014	0
CSK	30	04	2014	-863
CSK	08	05	2014	565
CSK	16	05	2014	372
CSK	01	06	2014	134
CSK	09	06	2014	713
CSK	25	06	2014	-586
CSK	03	07	2014	-1169
CSK	29	09	2014	-1168
CSK	07	10	2014	-668
CSK	15	10	2014	-410
CSK	23	10	2014	152
CSK	31	10	2014	-727
CSK	08	11	2014	329
CSK	24	11	2014	-780
CSK	02	12	2014	-924
CSK	10	12	2014	51
CSK	18	12	2014	243
CSK	26	12	2015	-216
CSK	03	01	2015	583
CSK	12	01	2015	380
CSK	19	01	2015	-989
CSK	27	01	2015	-1065
CSK	04	02	2015	-480
CSK	20	02	2015	-774
CSK	28	02	2015	-185
CSK	17	03	2015	147
CSK	08	09	2015	-694
CSK	16	09	2015	-187

Table 2: CSK SAR Acquisition list (cnd)

Mission	Day	Month	Year	Perpendicular Baseline [m]
CSK	24	09	2015	89
CSK	02	10	2015	-1018
CSK	18	10	2015	-35
CSK	11	11	2015	169
CSK	19	11	2015	-154
CSK	28	11	2015	-896
CSK	13	12	2015	115
CSK	29	12	2015	-1133
CSK	06	01	2016	-87
CSK	14	01	2016	-300
CSK	22	01	2016	19
CSK	30	01	2016	-863
CSK	07	02	2016	-269
CSK	15	02	2016	-141
CSK	23	02	2016	-474
CSK	02	02	2016	-682
CSK	10	03	2016	250
CSK06	18	03	2016	354

two relevant satellite heading angles. We can observe that SAR satellites orbits are near-polar circular and sun-synchronous, accordingly the sensitivity of SAR measurements to North-South deformation components (see Equation 1) is rather limited. Furthermore, previous studies on ocean-reclaimed platforms [14,20,50] suggest that the deformation is almost vertical, being the settlement mostly due to soil compaction mechanisms that are mainly responsible for vertical movements. For this reason, in this study we have assumed the reliability of the condition $\|\mathbf{E}^{(j)}\|_2 \ll \|\mathbf{H}^{(j)}\|_2$, $j = 1, 2$ stating that the two-norm of the East-West deformation vector is negligible with respect to the corresponding vertical one. Taking into account these assumptions, the time-series of vertical deformation components can be derived from LOS measurements as:

$$\mathbf{h}^{(i)} \approx \frac{\mathbf{d}^{(i)}}{\cos \vartheta^{(i)}} \quad i = 1, 2; \forall P \in S \quad (2)$$

Note that the vertical deformations $\mathbf{h}^{(j)}(P)$ $j = 1, 2; \forall P \in S$ (as individually retrieved by the two radar systems) are only known in relative with respect to their inherent first time epochs, i.e., $h_1^{(j)} = 0$, $j = 1, 2$. However, since we are interested in obtaining a unique deformation time-series of the vertical deformation components, namely $\mathbf{H} \equiv [H_1, H_2, \dots, H_{N_1+N_2}]^T \quad \forall P \in S$, that span the whole set of available time acquisitions $\mathbf{T} \equiv \mathbf{t}^{(1)} \sqcup \mathbf{t}^{(2)}$, we have to estimate the vertical deformation values at the two (initial) reference time epochs of each SAR dataset, namely $\hat{H}_{ENV} \equiv H|_{t=t_1^{(1)}}$ and $\hat{H}_{CSK} \equiv H|_{t=t_1^{(2)}}$. As a matter of fact, we have considered as a global reference the time at which the oldest SAR scene (as a whole) was acquired (i.e., in our case on February 26, 2007), thus we have imposed that the (vertical) deformation at that time was equal to zero (i.e., $\hat{H}_{ENV} = 0$). In such a way, linking CSK and ASAR/ENVISAT vertical time-series simply reduces to the estimation of one remaining (unknown) value of deformation (vertical component), which represents the displacement related to the first time epoch $t_1^{(2)}$ of the CSK SAR dataset, calculated relative to the time $t_1^{(1)}$ taken as global reference. Hence, the only unknown of the problem at hand becomes $\hat{H}_{CSK} \equiv H|_{t=t_1^{(2)}}$. Indeed, the CSK (vertical) DInSAR deformation time-series are completely known, but only relative to the inherent first CSK time epoch $t_1^{(2)}$; accordingly, the combined (unique) vertical deformation time-series can be written as:

$$H_j = H(T_j) = \begin{cases} h^{(1)}(T_j) & T_j < t_1^{(2)} \\ h^{(2)}(T_j) + \hat{H}_{CSK} & T_j \geq t_1^{(2)} \end{cases} \quad j = 1, \dots, N_1 + N_2 \quad (3)$$

In order to retrieve the combined (vertical) displacement time-series, we start by observing that the CSK dataset is completely non-time-overlapped to the ASAR/ENVISAT one. Accordingly, the time gap between the two SAR datasets makes the use of SVD, as done in the original SBAS algorithm [28], totally unreliable. In addition, the deformation over ocean-reclaimed platforms is known to be mostly non-linear in time, thus the simple option to extrapolate linear rate from ASAR/ENVISAT time series and use that value for the displacement at the first time epoch of the CSK time series reveals unreliable. For this reason, we have developed an “*ad-hoc*” method for circumventing that problem. The method is hereinafter detailed.

The basic idea is to exploit the knowledge of an external model of the deformation, which analytically describes how the deformation is expected to evolve over time. In particular, we focused on the ocean-reclaimed platforms of the Lingang New City (Shanghai), for which the mathematical expression of a time-dependent geotechnical model (derived from laboratory centrifuge tests) is available in the literature [44].

Then, the problem at hand can be mathematically formulated as follows. If a (non-linear) time-dependent model for the on-going deformation, calculated over the time vector $\tilde{\mathbf{T}} \equiv [0, T_1 - T_0, \dots, T_{W-1} - T_0]^T$ and with Q independent variables (e.g., $\alpha_1, \alpha_2, \dots, \alpha_Q$), namely $\mathbf{m} = \mathbf{m}(\mathbf{T}, \alpha_1, \alpha_2, \dots, \alpha_Q)$, is known, then the model that best fits the DInSAR measurements is the one that solves the following non-linear optimization problem:

$$\alpha_1, \alpha_2, \dots, \alpha_Q, \hat{H}_{CSK} = \arg \min [\|\mathbf{m} - \mathbf{H}\|_2] \quad (4)$$

where the symbol $\|\cdot\|_2$ stands for the two-norm of a vector. In particular, in the specific case of the Lingang New City in Shanghai, we have considered a (simplified) time-dependent geotechnical model (as derived from laboratory centrifuge tests), which is specifically intended for the ocean-reclaimed platforms of Shanghai, and depends on four distinctive variables. In particular, the model is given by [6],[44]:

$$\mathbf{m} = \mathbf{m}(\tilde{\mathbf{T}}, S, k, \lambda, \delta) = S \frac{(\tilde{\mathbf{T}} - \delta)^\lambda}{k^\lambda + (\tilde{\mathbf{T}} - \delta)^\lambda} \quad (5)$$

where S is the asymptotic value of vertical deformation (theoretically assumed at time infinite from now), k, λ are two parameters that control the shape of a given curve among the family of all the possible curves, and δ is a time-delay that takes into account the uncertainty in the knowledge of the exact time when reclamation processes ceased and the self-weight soil consolidation phase started [6]. Note that in Equation (5) the condition $|\tilde{\mathbf{T}} - \delta| \geq 0$ has implicitly been assumed, since the model only describes the soil compaction mechanisms, and thus it is only valid after the end of the reclamation processes. The time-dependent behavior of the adopted model was retrieved from laboratory tests that simulate, in a reduced scale, the real scenarios, and the kinematic parameters can be related to dredger-fill soil characteristics (i.e., thickness, water content, void ratio). For additional information, see also [46, 50, 57].

Finally, we observe that the proposed combination methodology is general, and it is particularly appropriate in the presence of non-linear deformation signals and/or when other external information is not available, and/or when the spatial sampling of the measurement points (for instance derived from GPS/leveling campaigns) is not adequate enough for linking time-gapped SAR data.

4. Experimental Results

We present in this Section the results of our joint C-/X- band investigation relevant to the coastal area of Shanghai, which has been performed using archived ASAR/ENVISAT and COSMO-SkyMed SAR images. The available data were processed through the advanced multi-temporal SBAS-DInSAR algorithm [28] that relies on selecting pairs of SAR acquisitions characterized by a short temporal (i.e., the time interval between two acquisitions) and spatial (i.e., the distance between two satellite passes) baselines in order to mitigate noise effects [58]. In particular, we have selected SAR data pairs with a perpendicular baseline < 800 m and a temporal baseline < 400 days and generated $M_1 = 91$ and $M_2 = 155$ interferograms from the ASAR/ENVISAT and CSK datasets, respectively. Selected SAR data-pairs are pictorially represented in the temporal/perpendicular baseline plane of Figure 2(a)-(b) as segments connecting SAR data acquisition points. The interferograms have been generated by computing the phase difference between the co-registered SAR image pairs [59], and by subtracting the relevant topographic phase contributions as synthesized using the Shuttle Radar Topography Mission (SRTM) DEM (with a spatial sampling of

90 x 90 meters) of the area [60]. Moreover, in order to mitigate the effects of the decorrelation noise, we independently carried out (on each single interferogram) a complex multilook operation [61] (with 30 looks in the azimuth and range directions for the CSK case, and with 20 looks in the azimuth and 4 looks in the range direction for the ASAR/ENVISAT case, thus resulting for both SAR datasets in a radar pixel dimension of about 90 m x 90 m). Subsequently, on each interferogram a noise-filtering operation [62] was applied. Figure 3 shows four differential SAR interferograms with different spatial and temporal baseline values. Note that the temporal decorrelation noise artifacts corrupt the interferograms as the temporal baseline increases, and this effect is more accentuated in the coastal area. Moreover, as expected, the observed temporal decorrelation is generally more severe at X-band than at C-band [39].

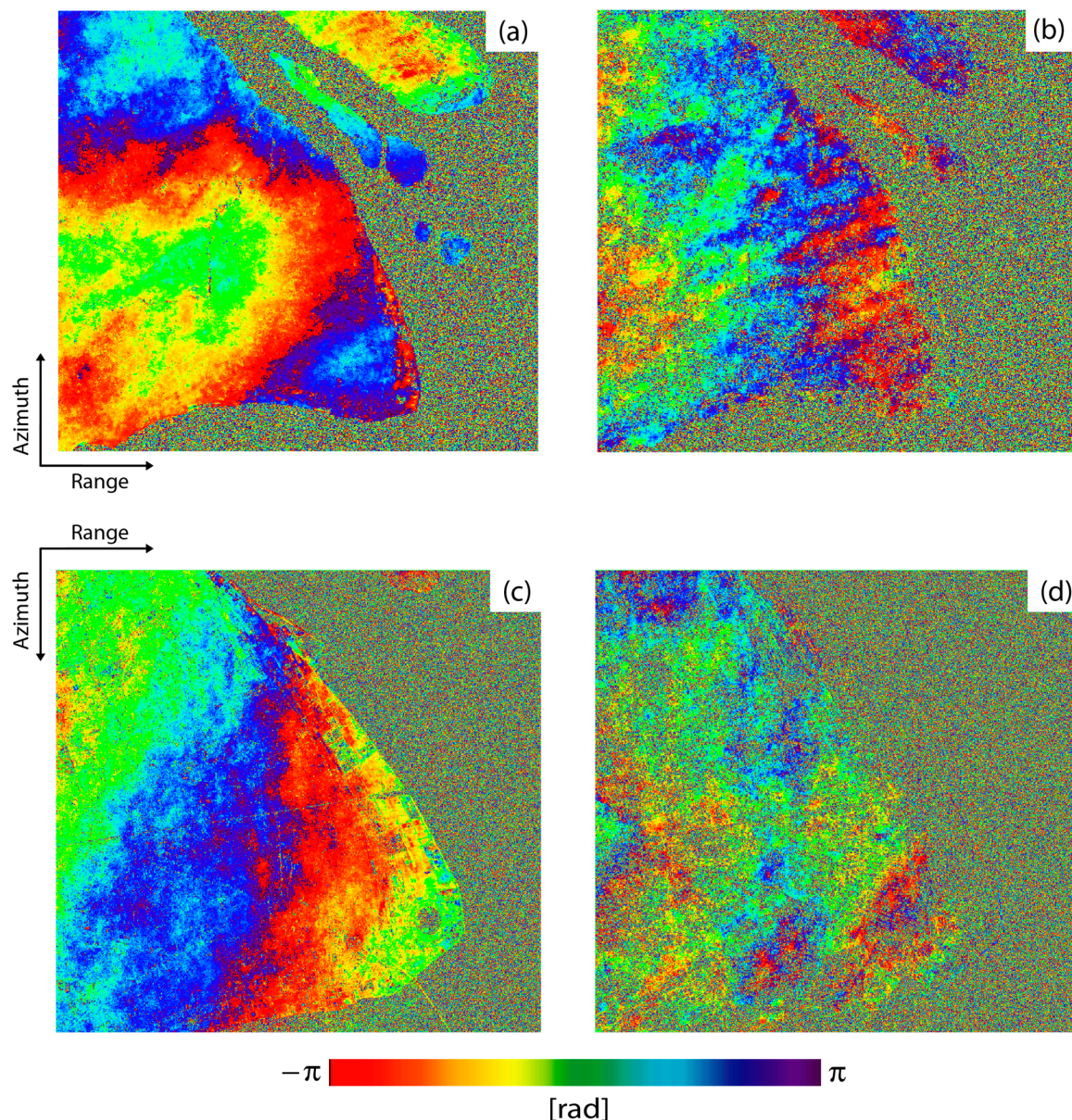


Figure 3. Four selected DInSAR interferograms relevant to the Shanghai area, achieved by exploiting ENVISAT/ASAR acquisitions over ascending orbits (a-b) and CSK SAR data over descending orbits (c-d). (a) 29 October 2007 – 3 December 2007 ENVISAT interferogram with perpendicular baseline of about 64 m. (b) 2 March 2009 – 20 July 2009 ENVISAT interferogram, 5 m of perpendicular baseline. (c) 8 January 2014 – 9 February 2014 CSK interferogram with perpendicular baseline of 70 m. (d) 27 January 2015 – 2 October 2015 CSK interferogram, 45 m of perpendicular baseline. The spatial coherence in (b) and (d) is not preserved in correspondence to the reclaimed area of Lingang New City, due to the large

temporal baseline values of these SAR data pairs despite the overall short spatial baseline values, resulting in the temporal decorrelation noise artifacts.

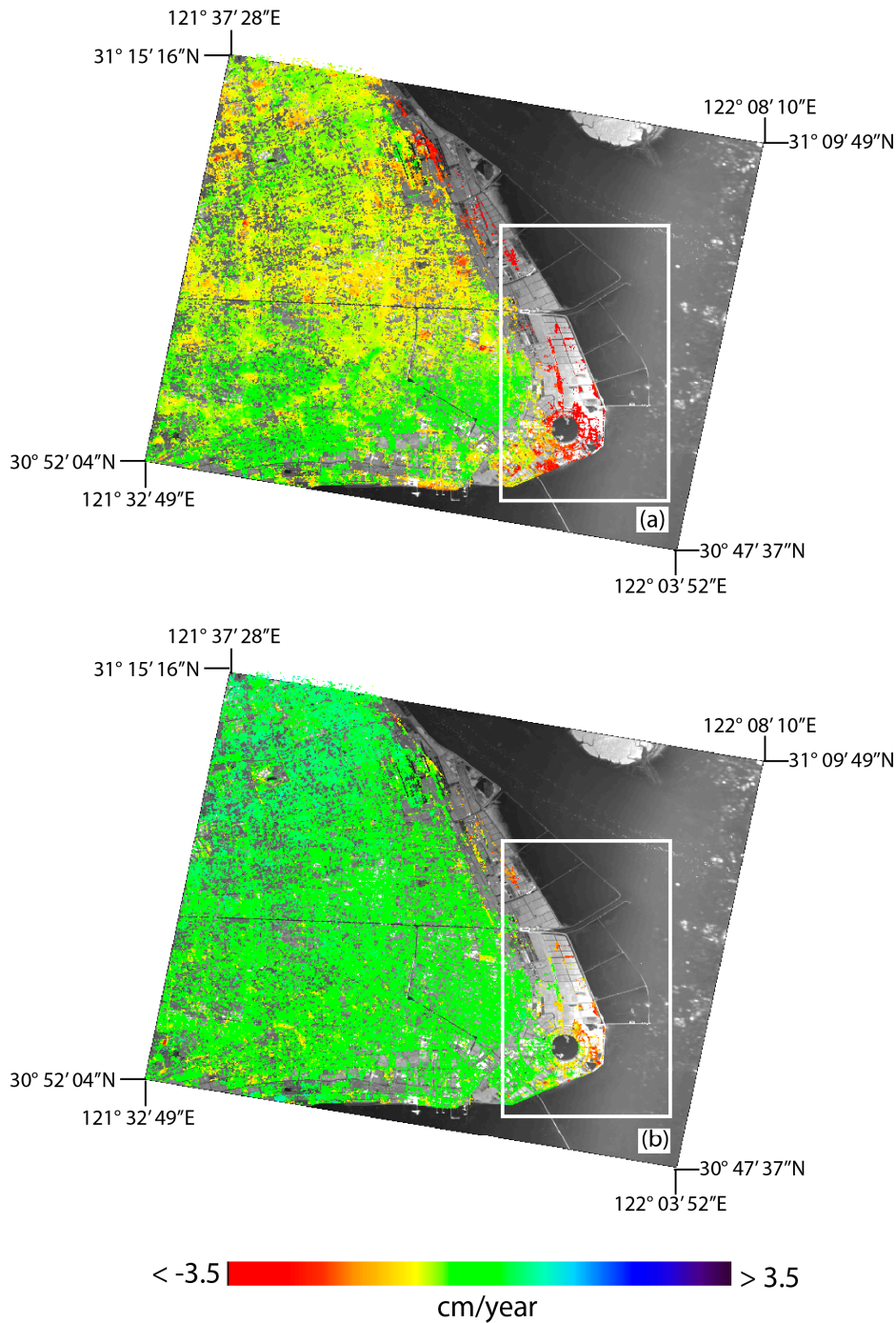


Figure 4. LOS SBAS-DInSAR mean displacement velocity maps retrieved using the 2007-2010 ASAR/ENVISAT (a) and the 2014-2016 CSK (b) datasets, and represented on the common geocoded grid. The white rectangles represent the reclaimed area of Lingang New City, where the following comparative analysis has been performed.

Then, the generated differential SAR interferograms, say $\Delta\phi^{(j)} \equiv [\Delta\phi_1^{(j)}, \Delta\phi_2^{(j)}, \dots, \Delta\phi_{M_j}^{(j)}]^T$ $j = 1, 2$ have been unwrapped. The phase unwrapping (phU) operations have been carried out, separately for the two available sets of interferograms, by applying the Extended Minimum Cost Flow (EMCF)

algorithm [63-64]. We remark that the EMCF phU algorithm is a hybrid space-time approach consisting in a two-step processing procedure, whose rationale is rather simple. First, a Delaunay triangulation is built in the azimuth/range radar domain, involving the sparse set of the coherent pixels, and subsequently, for each arc of the spatial Delaunay triangulation, a “temporal” phU step is performed [63]. Both the temporal and spatial phU steps are based on the application of the minimum cost flow (MCF) phU principles [65]. The two sets of unwrapped interferograms are then eventually (independently for the two SAR datasets) inverted through the SBAS technique [28]. During the processing, residual topographic artifacts as well as the atmospheric phase screen signal are estimated and filtered out. Interested readers can find additional details on the used SBAS processing chain in [66-67].

As a result of the application of the SBAS technique, we have obtained (for each coherent target of the radar scene common to the two available SAR datasets) the relevant LOS displacement time-series, $\mathbf{d}^{(j)}$ $j=1,2$ which have subsequently been geocoded. Furthermore, the quality of achieved results is checked, pixel-by-pixel, by measuring the temporal coherence value. It is worth remarking that the temporal coherence [63] essentially gives a figure about phase unwrapping errors committed during the processing. Then, all the pixels exhibiting temporal coherence values smaller than a specific threshold (in particular, in our experiment we have used for both the datasets the value of 0.65) are discarded. Figure 4 shows the two maps of the mean displacement velocities depicted on the two inherent sets of (geocoded) coherent pixels for the ASAR/ENVISAT (2a), and the CSK (2b) datasets, respectively, properly superimposed on an amplitude SAR image of the investigated area.

Finally, in order to retrieve a unique deformation time-series of vertical components that span the entire time period covered by the two available SAR datasets (from February 2007 to March 2016) we have applied the combination methodology discussed in Section 3.

5. Discussion

In this Section, we analyze the achieved SBAS results in relation to the characteristic of deformation signals in the ocean-reclaimed platforms of Shanghai. In particular, we provide additional details on the non-linear time-dependent model used for the combination of CSK and ASAR/ENVISAT displacement time-series, and we check and discuss the quality of the non-linear optimization procedures adopted for combining the two InSAR datasets. Finally, a comparative analysis between the newly derived and the old models as well as a discussion on the main outcomes of the work is provided.

First, we focus on the detected deformation signals and we spend a few additional words about the assumption on negligibility of East-West component of the surface displacement with respect to vertical (subsidence/uplift) one. We remark that such an assumption is valid in ocean-reclaimed platforms but it is not generally met everywhere in the overall Shanghai megacity area. Indeed, the southwestern sector of the Shanghai area has recently claimed to be crossed by a geological fault, the so-called Dachang-Zhoupu fault (see the black line in Figure 1), which is responsible for appreciable deformation movements in that sector of the city also along the East-West direction (with magnitude however less than 1 cm/year with respect to a reference point located in correspondence to the GPS station labeled to as SHAO in Figure 1). Such displacements were measured in the period from 2002 to 2005 through a network of 17 GPS stations (see [68] for the location of the GPS stations and their relative movements), and were related to the neo-tectonic activity of an existing geological fault [68-69]. Nevertheless, there is no direct evidence that these East-West deformations also extend up to the areas in reclamation, located South-East of Shanghai, where it is known that deformations are dominated by soil-compaction mechanisms, which are primarily responsible for vertical movements. For this reason the additional contributions to settlement due to fault mechanisms have been assumed negligible in our study. We finally point out that despite the fact that ASAR/ENVISAT and CSK data have been acquired through ascending and descending passes, respectively, they

cannot be combined to extrapolate the East-West and Up-Down components of deformations since they do not span the same time-period of observation.

Second, for what attains the used model in Equation (5), we remark that it is derived from laboratory tests aimed at assessing, for instance, the stability and capacity of building foundations. Its basic principle is to recreate the conditions that would exist in a full-scale construction by using a model on a reduced scale. Centrifuge model testing provides researchers with simulated data that are able to improve the understanding of basic mechanisms of deformation, allowing the retrieval of experimental data for the verification of numerical models. Of particular interest, due to the peculiar alluvial soil characteristics of Shanghai, is the model settlement retrieved in [44], which permits to analyze ground settlement caused primarily by self-weight consolidation mechanisms. The simplified model in [44] can be derived from the general model described in [50] and those presented in [57], which relate kinematic parameters to physical soil characteristics.

The non-linear optimization problem in Equations (4)-(5) has efficiently been solved via the (iterative) Levenberg-Marquadt least squares (LS) minimization technique [70-71], as provided in the implementation of the MPFIT module, which is available in several programming languages. In particular, for our experiments, we have used the code implemented in the MPFIT module available in the Interactive Data Language (IDL) language environment [72].

At this stage, we analyze the achieved results by specifically focusing on the ocean-reclaimed area of the Lingang New City. Figure 5(a) shows a zoomed view of the map reporting the mean displacement rate of the vertical deformation in the Lingang New City area, as retrieved by combining the ASAR/ENVISAT and CSK data. As earlier said, the multi-platform time-series combination has been performed by searching for the model parameters as well as for the (unknown) bias between the ASAR/ENVISAT and the CSK time-series that best fit the data. More precisely, for each coherent target common to both datasets, we have searched for the best-fit curve in the LS sense between the model and the DInSAR deformation, by solving the problem in Equations 4 and 5. Subsequently, we have also checked the quality of the nonlinear curve fitting by calculating the root mean square error (RMSE) of the difference between the (reconstructed) DInSAR-based (vertical) deformation time-series and the obtained best-fit model. The map of the RMSE values is shown in Figure 5(b). By inspecting Figure 5(b), it is evident that the obtained RMSE is on average on the order of a few millimeters. Table 3 also reports the (average) RMSE values calculated over the areas of the Lingang New city in its eastern (ES) and western (WS) sectors, respectively, as retrieved from the combined ENVISAT/CSK (vertical) deformation time-series. Besides, we have repeated the RMSE calculation by considering the fitting between the obtained models and the ASAR/ENVISAT and CSK time-series, separately. The achieved results are summarized in Table 3.

Table 3. Average RMSE values between the DInSAR time-series and the recovered best-fit models for the Western (WS) and the Eastern (ES) sectors.

Sensor	WS	ES
ENVISAT	5.8 mm	8.0 mm
CSK	3.4 mm	5.7 mm
ENVISAT/CSK	4.8 mm	7.2 mm

We remark that the best-fit models retrieved as the result of the combination of C/X-band displacement time-series are in general agreement with the forecast models studied in our previous investigation [19], which was exclusively based on the use of ASAR/ENVISAT data. Moreover, it is worth noting that newly CSK deformation time-series distinctly evidence that the rate of deformation in ocean-reclaimed platforms has progressively been decreasing over the recent six years, following a decay rule that is in general accordance with the time-dependency of the models in (5). This is confirmed also by the temporal shape of the individual ASAR/ENVISAT and the CSK time-series as well as by the plots of the combined (vertical) deformation time-series. In particular, Figure 5 shows the deformation time-series relevant to four selected pixels, labeled to as P₁, P₂, P₃

and P4. Table 4 lists the best-fit model parameters retrieved for these four selected points. We remark that these pixels have been selected among the ones characterized by the smallest values of the RMSE (which is indicated for all the four pixels in the relevant plot of Figure 5) as representative of the (average) present-state of residual settlement due to consolidation of soils in the different zones of the Lingang New City.

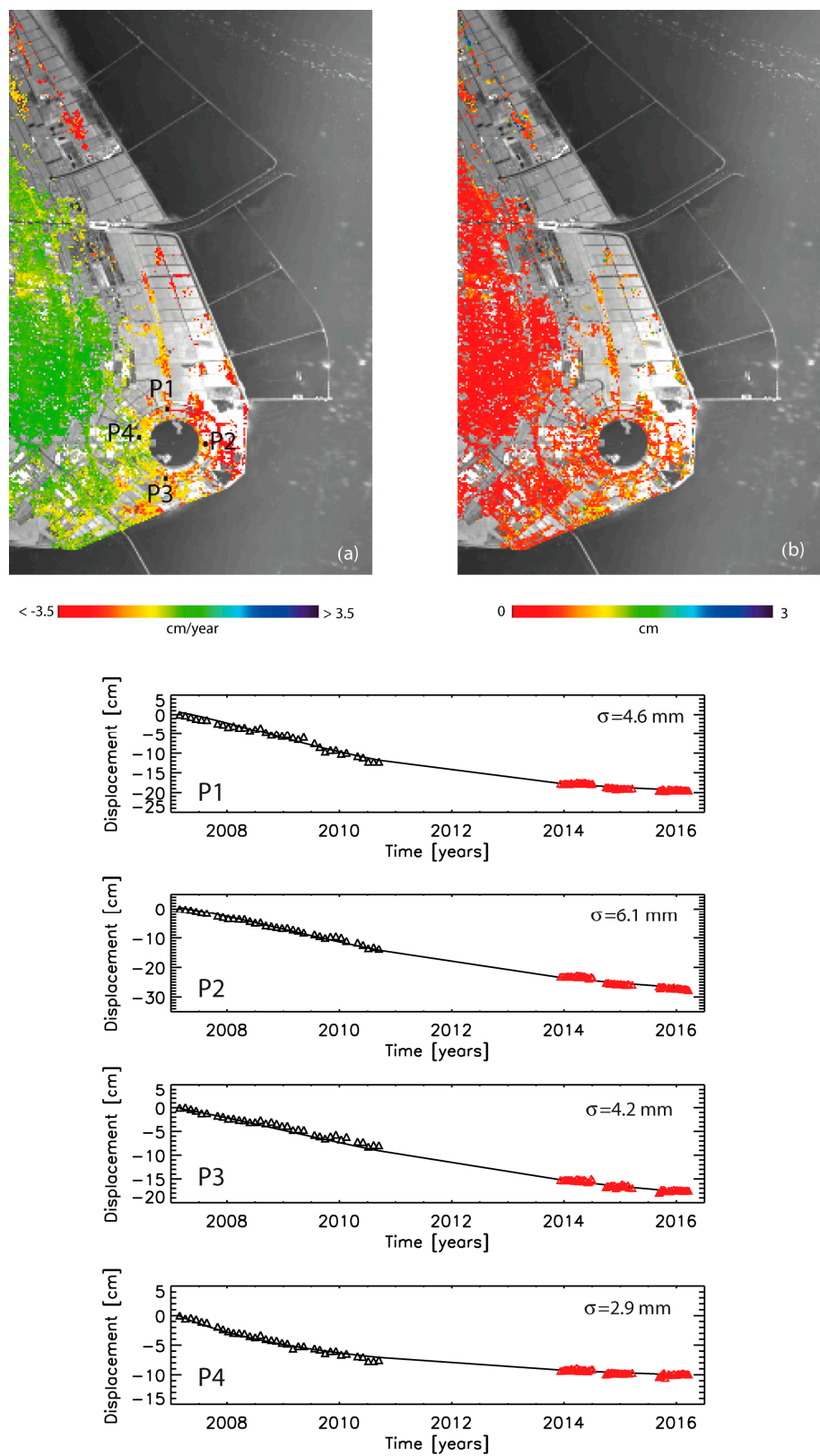


Figure 5. (a) Geocoded map of the mean (vertical) velocity deformation occurred during the 2007-2016 time-interval over the Lingang New City, as retrieved by combining ENVISAT and CSK LOS displacement time-series. (b) Map in false color of the RMSE values of the difference between the computed best-fit models and the combined ENVISAT/CSK (vertical) deformation time-series. The plots of the ASAR/CSK combined (vertical) deformation time-series computed in correspondence to four pixels labeled to as P₁, P₂, P₃ and P₄ are also shown. Combined time-series are plotted with black (ASAR/ENVISAT) and red (CSK) triangles, whereas the corresponding best-fit models are plotted with continuous black lines.

Table 4. Values of the best-fit model parameters retrieved for the four selected points of Figure 5(b).

Point	S [cm]	k	λ	δ *****
P1	-19.7	11.9	0.7	-5.
P2	-41.2	26.6	0.7	-3.
P3	-27.6	16.2	0.7	-1.
P4	-11.4	8.6	0.5	-4.

As evidenced in previous investigations, it is clear that the eastern part of the city, which is closer to the coast, is currently still affected by appreciable deformations, whereas the western sector of the city is at present-days, after about ten years from the end of the reclamation processes [19], almost stable.

One of the outcomes of our previous investigation was the recovery of some preliminary predictions of the cumulative displacements in the ocean-reclaimed platforms of Shanghai by the end of 2015, 2020 and 2025 (see Figure 8 of [19]), calculated by considering as starting time for the soil consolidation phase the end of reclamation procedures, occurred depending on the site location beginning from 2006. One goal of the present analysis is to confirm/corroborate our previous results taking into account the “temporal shape” of (vertical) deformation time-series in the recent years (from 2013 to 2016) as captured by the CSK constellation sensors. As a matter of fact, the comparison between the “predicted” cumulative displacement maps related to the year 2015 and the one obtained in March 2016 (see Figure 6) by combining ASAR/ENVISAT and CSK time-series, shows that the newly acquired CSK data chiefly confirm the validity of previous best-fit models (see Figure 8 of [19] for a direct comparison). The deviation of the measured deformations from best-fit models as retrieved using only ASAR/ENVISAT data (covering the period from 2007 to 2010) and the ones retrieved now by using the combined CSK/ENVISAT data is minimal, as testified by the mean RMSE values listed in Table 5. The differences between the newly derived and the old models are more appreciable in the eastern sector of the city than in the western part. This is due to the different type of used soils and to the different stages of soil consolidation that the two areas are experiencing.

Table 5. Average RMSE values of the difference between the best-fit models retrieved by using only ENVISAT data (2007-2010) and the ones retrieved from the combined ENVISAT/CSK data (2007-2016). RMSE values are have been computed for both the Western and the Eastern sectors of Lingang New City.

Sensor	WS	ES
ENVISAT vs. ENVISAT/CSK	3.9 mm	6.4 mm

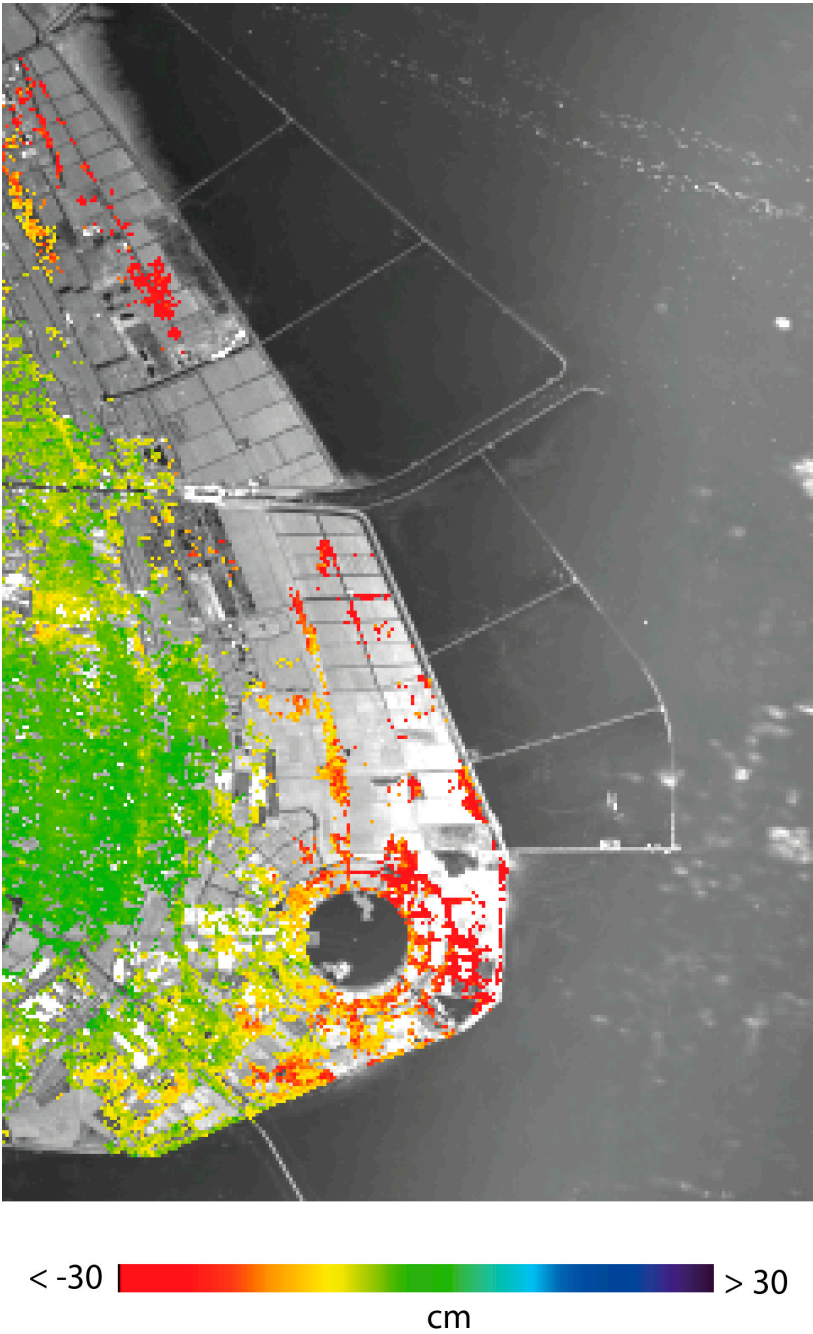


Figure 6. Map of the whole cumulative displacement at March 18, 2016, as obtained by the combination of ASAR/ENVISAT and the CSK time-series.

6. Conclusions

An up-to-date investigation of the residual deformation of ocean-reclaimed platforms over the coastal area of the Shanghai megacity, as recovered by properly combining DInSAR-driven time-series of deformation obtained at the different (C and X) frequency bands, has been provided in this work. In particular, we have processed ENVISAT/ASAR (C-band) and CSK (X-band) radar images acquired from 2007 to 2016. The achieved DInSAR deformation time-series have then jointly been integrated by taking profit from the knowledge of a geotechnical time-dependent model, derived from laboratory centrifuge tests, for the deformations occurring in the area under investigation. In particular, in this work we have used such models to further extend some previous analyses [19]. As a result, we have shown there is a good agreement in shape between the combined-C/X-band DInSAR (vertical) time-series and what theoretically expected by the model,

itself. The newly processed CSK time-series show that deformation in ocean-reclaimed platforms has progressively been decaying over time, and the areas that were firstly reclaimed are today (after almost ten years by the end of reclamation procedures) rather stable. On the contrary, the eastern sector of the Lingang New City, where the reclamation procedures started later, is still today affected by significant deformation signals, although their rate is gradually reducing over time.

The method we have used to link time-gapped displacement time-series relies on the knowledge of a model for the expected deformation and on the hypothesis that deformation over reclaimed platforms is mostly vertical. The latter hypothesis is reasonable since the soil consolidation stages as well as the mechanisms induced by the weight of the buildings, which have been built in the new city, are at most responsible for vertical movements of the terrain. Nonetheless, the lack of sufficiently large archives of time-overlapped ascending/descending SAR images over the Lingang New City (just in correspondence to reclaimed areas) has made unreliable the measurement of the East-West deformation rates directly from SAR data, as provided for instance by using the methods in [73-79]. Moreover, such a strategy can generally be extended in other cases where deformation components in East-West directions cannot be considered negligible, by profitably combining the strategies here adopted and the combination methods discussed in [73-79] that exploit SAR data acquired by multiple-sensors and different orbital positions (e.g., from ascending and descending passages).

We finally remark that in order to extend and fully validate our prediction models, we count to access in the near future to data gathered by a network of GPS that is currently being deployed in the Lingang New City, and to make use of the archives of newly acquired SAR data collected by the European Sentinel-1A/B C-band SAR sensors of the Copernicus programme [80]. In fact, at the time of this investigation Sentinel archives relevant to the area under investigation were not sufficiently populated (less than 20 scenes) to allow the generation of reliable and steady displacement time-series. Their use is matter for further studies and investigations.

Acknowledgments: This work has been carried out within the Dragon III ESA project ID 10644 entitled “DInSAR Detection of Surface Deformation in the Coastal Reclaimed Areas of Shanghai City.” Cosmo-SkyMed SAR data were provided to us by the Italian Space Agency (ASI) in the framework of the mentioned Dragon III project, whereas ENVISAT/ASAR data were provided by European Space Agency (ESA) in the framework of the CAT-1 ESA nr. 11461 project. This work was supported by Research Grants of Science and Technology Commission of Shanghai Municipality through Project 13ZR1453900 and 13231203804, by the High-End Foreign Experts Recruitment Program of the State Administration of Foreign experts Affairs through Project GDW20143100087, and by the I-AMICA project of structural improvement financed under the National Operational Programme (PON) for “Research and Competitiveness 2007–2013,” co-funded with the European Regional Development Fund (ERDF) and National Resources. The authors would also like to acknowledge the contribution of Simone Guarino, Maria Consiglia Rasulo and Fernando Parisi for their valuable technical support. We also thank the anonymous reviewers for their valuable comments and suggestions.

Author Contributions: Antonio Pepe developed the combination method and supervised the research and the algorithm development; he also prepared the manuscript. Manuela Bonano computed the ASAR/ENVISAT and the CSK DInSAR time-series and revised the manuscript. Qing Zhao contributed to the preparation of the manuscript and provided information for the geophysical assessment of the area. Tianliang Yang and Hamei Wang revised the whole manuscript and contributed by searching for the recent literature related to the area under investigation.

Conflicts of Interest: The authors declare no conflict of interest.

References

1. R. J. Hoeksema, "Three stages in the history of land reclamation in the Netherlands," *Irrigation and Drainage*, vol. 56, pp. 113–216, Dec. 2007.
2. I. Douglas, N. Lawson, "Airport construction: materials use and geomorphic change," *Journal of Air Transport Management*, vol. 9, no. 3, pp. 177–185, May 2003.
3. Q. Zhao, H. Lin, W. Gao, H. Zebker, A. Chen, K. Yeung, "InSAR detection of residual settlement of an ocean reclamation engineering project: a case study of Hong Kong International Airport," *J. Oceanogr.*, vol. 67, no. 4, pp. 415–426, Aug. 2011.
4. D. Ganesalingam, J. Ameratunga, G. Schweitzer, P. Boyle, S. Sivakugan, "Anisotropy in the permeability and consolidation characteristics of dredged mud," in *Proc. ANZ 2012, Ground Engineering in a Changing World: 11th Australia - New Zealand Conference on Geomechanics*, 2012, pp. 752–757.
5. D. R. E. Philip, J. D. McIlquham, "Geotechnical design for the Port Botany expansion project," in *Proc. the ICE - Geotechnical Engineering*, 2011, pp. 149–167.
6. A. M. Puzrin, E. E. Alonso, N. M. Pinyol, "Unexpected Excessive Settlements: Kansai International Airport, Japan," in *Geomechanics of Failures*, Springer, 2010, pp. 23–43.
7. A. Rizzo, "Metro Doha," *Cities*, vol. 31, pp. 533–543, Apr. 2013.
8. H. Yang, "Legal Regulation of Land Reclamation in China's Coastal Area," *Coast. Manage.*, vol. 42, no. 1, pp. 9–79, Jan. 2014.
9. Y.H. Yin, "Thinking on large area reclamation in Caofeidian, Tangshan city, Hebei Province.," *Marine Geology Letters*, vol. 23, no. 3, pp. 1–10, Dec. 2007.
10. Z. Y. Wang, Y. Li, Y. He, "Sediment budget of the Yangtze River," *Water Resour. Res.*, vol. 43, pp. 1–14, Apr. 2007.
11. Liu, G.X.; Luo, X.J.; Chen, Q.; Huang, J.F.; Ding, X.L. Detecting land subsidence in Shanghai by PS-networking SAR interferometry. *Sensors* 2008, 8, 4725–4741.
12. S. Bhattacharyaa, M. Hyodob, K. Godaa, T. Tazohc, C.A. Taylora, "Liquefaction of soil in the Tokyo Bay area from the 2011 Tohoku (Japan) earthquake," *Soil Dynamics and Earthquake Engineering*, vol. 31, no. 11, pp. 1618–1628, Nov. 2011.
13. L. K. Chien, Y. N. Oh, C. H. Chang, "Effects of fines content on liquefaction strength and dynamic settlement of reclaimed soil," *Can. Geotech. J.*, vol. 39, no.1, pp.254–265, Oct. 2002.
14. G. W., C. S. Covil, and R. A. Hughes, "Geology, Surveying, Reclamation Settlement," in *Site Preparation of the New Hong Kong International Airport*, 1st ed. London, UK: Thomas Telford, 1998, pp. 45, 387–416, 515–517.
15. M.-S. Yang, Y. Jiang, M. Liao, and H. Wang, "The analysis of the subsidence patterns in Lingang New City (Shanghai) using high-resolution SAR images," *Shanghai Land Resour.*, vol. 34, no. 4, pp. 12–16, Jun. 2013 (in Chinese).
16. J. Chen, J. Wu, L. Zhang, J. Zou, G. Liu, R. Zhang and B. Yu, "Deformation Trend Extraction Based on Multi-Temporal InSAR in Shanghai," *Remote Sens.* 2013, 5, 1774–1786.
17. D. Perissin, Z. Wang, H. Lin, "Shanghai subway tunnels and highways monitoring through Cosmo-SkyMed Persistent Scatterers," *ISPRS Journal of Photogrammetry and Remote Sensing* 73 (2012) 58–67.
18. S. Dong, S. Samsonov, H. Yin, S. Y, Y. Cao, "Time-series analysis of subsidence associated with rapid urbanization in Shanghai, China measured with SBAS InSAR method," *Environ Earth Sci* (2014) 72:677–691.
19. Q. Zhao, A. Pepe, W. Gao, Z. Lu, M. Bonano, M. L. He, J. Wang, and X. Tang, "A DInSAR Investigation of the Ground Settlement Time Evolution of Ocean-Reclaimed Lands in Shanghai," *IEEE Selected Topics in Applied Earth Observations and Remote Sensing*, vol.8, no 4,1763–1781.
20. K. Been and G. C. Sills, "Self-weight consolidation of soft soils: An experimental and theoretical study," *Geotechnique*, vol. 31, no. 4, pp. 519–535, 1981.
21. K. Terzaghi, P. B. Ralph, M. Gholamreza, *Soil Mechanics in Engineering Practice*, 3rd ed., Hoboken, Wiley-Interscience, 1996, pp. 1–592.

22. R. Bürgmann, P. A. Rosen, and E. J. Fielding, "Synthetic aperture radar interferometry to measure Earth's surface topography and its deformation," *Annu. Rev. Earth Planet. Sci.*, vol. 28, pp. 169–209, May 2000.
23. D. Massonnet and K. L. Feigl, "Radar interferometry and its application to changes in the Earth's surface," *Rev. Geophys.*, vol. 36, pp. 441–500, 1998.
24. D. Massonnet et al., "The displacement field of the Landers earthquake mapped by radar interferometry," *Nature*, vol. 364, pp. 138–142, Jul. 1993.
25. D. Massonnet, P. Briole, and A. Arnaud, "Deflation of Mount Etna monitored by spaceborne radar interferometry," *Nature*, vol. 375, pp. 567–570, Jun. 1995.
26. A. Ferretti, C. Prati, and F. Rocca, "Permanent scatterers in SAR interferometry," *IEEE Trans. Geosci. Remote Sens.*, vol. 39, no. 1, pp. 8–20, Jan. 2001.
27. B. M. Kampes, *Radar Interferometry: Persistent Scatterer Technique*. New York, NY, USA: Springer, 2006.
28. P. Berardino, G. Fornaro, R. Lanari, E. Sansosti, "A new algorithm for surface deformation monitoring based on small baseline differential SAR interferograms," *IEEE Trans. Geosci. Remote Sens.*, 2002, 40, 2375–2383.
29. O. Mora, J. J. Mallorquí, and A. Broquetas, "Linear and nonlinear terrain deformation maps from a reduced set of interferometric SAR images," *IEEE Trans. Geosci. Remote Sens.*, vol. 41, no. 10, pp. 2243–2253, Oct. 2003.
30. S. Usai, "A least squares database approach for SAR interferometric data," *IEEE Trans. Geosci. Remote Sens.*, vol. 41, no. 4, pp. 753–760, Apr. 2003.
31. G. Strang, *Linear Algebra and Its Applications*. Orlando, FL, USA: Harcourt Brace Jovanovich, 1988.
32. A. Hooper, D. Bekaert et al., "Recent advances in SAR interferometry time series analysis for measuring crustal deformation," *Tectonophysics*, vol. 514, pp. 1–13, Jan. 2012.
33. M. Neri, F. Casu, V. Acocella, G. Solaro, S. Pepe, S. P. Berardino, E. Sansosti, T. Caltabiano, P. Lundgren, R. Lanari, "Deformation and eruptions at Mt. Etna (Italy): A lesson from 15 years of observations," *Geophysical Research Letters*, vol. 36, Jan. 2009
34. Y. Yan, MP Doin, P. Lopez-Quiroz, F. Tupin, B. Fruneau, V. Pinel, E. Trouve, "Mexico City Subsidence Measured by InSAR Time Series: Joint Analysis Using PS and SBAS Approaches," *IEEE Journal Of Selected Topics In Applied Earth Observations and Remote Sensing*, Vol. 5, n°4, pp. 1312–1326, Aug. 2012.
35. R. Lanari et al., "Surface displacements associated with the L'Aquila 2009 Mw 6.3 earthquake (Central Italy): New evidence from SBASDInSAR time series analysis," *Geophys. Res. Lett.*, vol. 37, p. L20309, Oct. 2010.
36. E. Sansosti et al., "How second generation SAR systems are impacting the analysis of ground deformation," *Int. J. Appl. Earth Observ.*, vol. 28, no. 1, pp. 1–11, 2014, doi: 10.1016/j.jag.2013.10.007.
37. V. Greif, J. Vicko, "Monitoring of post-failure landslide deformation by the PS-InSAR technique at Lubietova in Central Slovakia," *ENVIRONMENTAL EARTH SCIENCES*, vol. 66, no. 6, pp. 1585–1595, Jul. 2012.
38. F. Guzzetti, M. Manunta, F. Ardizzone, A. Pepe, M. Cardinali, G. Zeni, P. Reichenbach & R. Lanari (2009), "Analysis of ground deformation detected using the SBAS-DInSAR technique in Umbria, Central Italy," *Pure and Applied Geophysics*, Vol. 166, doi: 10.1007/s00024-009-0491-4.
39. M. Bonano, M. Manunta, A. Pepe, L. Paglia, and R. Lanari, "From previous C-band to New X-band SAR systems: Assessment of the DInSAR mapping improvement for deformation time-series retrieval in urban areas," *IEEE Trans. Geosci. Remote Sens.*, vol. 51, no. 4, pp. 1973–1984, Apr. 2013.
40. I Parcharidis, E. Lagios, V. Sakkas, D. Raucoules, D. Feurer, S. Le Mouelic, C. King, C. Carnec, F. Novali, A. Ferretti, R. Capes, G. Cooksley, "Subsidence monitoring within the Athens Basin (Greece) using space radar interferometric techniques," *Earth Planet and Space*, vol. 58, no.5, pp. 505–513.
41. O. Cavalie, A. Sladen, M. Kelner, "Detailed quantification of delta subsidence, compaction and interaction with man-made structures: the case of the NCA airport, France," *Natural Hazards and Earth System Science*, vol. 9, pp. 1973–1984, 2015.
42. J.Z. Zhang, H. Hauang, H. Bi, "Land Subsidence in the modern Yellow River Delta based on InSAR time-series Analysis," *Natural Hazards*, vol. 75, no. 3, pp. 2385–2397, Feb. 2015
43. M. H. Aly, A. G. Klein, H. Zebker, "Land Subsidence in the Nile Delta of Egypt by persistent scatterer interferometry," *Remote Sensing Letters*, vol. 3, no. 7, pp. 621–630, 2012.

44. P. Yang, Y.-Q. Tang, N.-Q. Zhou, and J.-X. Wang, "Consolidation settlement of Shanghai dredger fill under self-weight using centrifuge modeling test," *J. Cent. South Univ. Technol.*, vol. 39, no. 4, pp. 862–866, Aug. 2008 (in Chinese).
45. R. N. Taylor, "Geotechnical Centrifuge Technology," Glasgow, U.K., Blackie Academic and Professional, 1995.
46. C. Zhen-Dong, T. Yi-Qun, "Land subsidence and pore structure of soils caused by the high-rise building group through centrifuge model test," *Engineering Geology*, vol. 113, pp.44-52.
47. Y.-S. Xu, L. Ma, Y.-J. Du, S.-L. Shen, "Analysis of urbanization-induced land subsidence in Shanghai," *Nature Hazards*, vol. 63, no. 2, pp. 1255–1267, Sep. 2012.
48. Shanghai Municipal Bureau of planning and land resources (SMBPLR), "Shanghai geological environmental bulletin (2001-2009)," 2009. (In Chinese).
49. S. L. Yang, J. D. Milliman, P. Li, K. Xu, "50,000 dams later: Erosion of the Yangtze River and its delta," *Global and Planetary Change* 75 (2011) 14–20.
50. Y. J. Zhou, X. He, P. Yang, J. Wang, "Theoretical and experimental study of consolidation settlement characteristics of hydraulic fill soil in Shanghai," *Environ Earth Sci.* DOI 10.1007/s12665-012-1584-4.
51. S. L. Shen, "Geological environmental character of Lin Gang New City and its influences to the construction," *Shanghai Geol.*, vol. 105, pp. 24–28, Dec. 2008 (in Chinese).
52. Y. Shi, X. Yan, and N. Zhou, "Land subsidence induced by recent alluvia deposits in Yangtze River delta area, a case study of Shanghai Lingang New City," *J. Eng. Geol.*, vol. 15, no. 3, pp. 391–402, Dec. 2007 (in Chinese).
53. Y. L. Desnos, H. Laur, P. Lim, P. Meisl, and T. Gach, "The Envisat-1 advanced synthetic aperture radar processor and data products," in *Proc. IGARSS, Hamburg, Germany, 1999*, pp. 1683–1685.
54. F. Covelto, F. Battazza, A. Coletta, E. Lopinto, C. Fiorentino, L. Pietranera, G. Valentini, and S. Zoffoli, "COSMO-SkyMed an existing opportunity for observing the Earth," *J. Geodyn.*, vol. 49, no. 3/4, pp. 171–180, Apr. 2010.
55. T. J. Wright, B. E. Parsons, and Z. Lu, "Toward mapping surface deformation in three dimensions using InSAR," *Geophys. Res. Lett.*, vol. 31, p. L01607, 2004, doi:10.1029/2003GL018827.
56. L. Gray, "Using multiple RADARSAT InSAR pairs to estimate a full three-dimensional solution for glacial ice movement," *Geophys. Res. Lett.*, vol. 38, no. 5, pp. L05502-1–L05502-6, Mar. 4, 2011.
57. G. W. Plant, C. S. Covil, R. A. Hughes, "Geology, surveying, reclamation settlement. In: Site preparation of the new Hong Kong International Airport," Thomas Telford, London, UK, pp 1°C45, 387°C416, 515°C517, 522 2009.
58. H. A. Zebker and J. Villasenor (1992) Decorrelation in interferometric radar echoes, *IEEE Trans. Geosci. Remote Sens.*, vol. 30, no. 5, pp. 950–959, Sep. 1992.
59. E. Sansosti, P. Berardino, M. Manunta, F. Serafino, and G. Fornaro, "Geometrical SAR image registration," *IEEE Trans. Geosci. Remote Sens.*, vol. 44, no. 10, pp. 2861–2870, Oct. 2006.
60. P. A. Rosen, S. Hensley, E. Gurrola, F. Rogez, S. Chan, and J. Martin, "SRTM C-band topographic data quality assessment and calibration activities," in *Proc. IGARSS, Sydney, Australia, 2001*, pp. 739–741.
61. P. A. Rosen, S. Hensley, I. R. Joughin, F. K. Li, S. N. Madsen, E. Rodriguez, and R. M. Goldstein, "Synthetic aperture radar interferometry," *IEEE Trans. Geosci. Remote Sens.*, vol. 48, no. 3, pp. 333–382, Mar. 2000.
62. R. M. Goldstein and C. L. Werner, "Radar interferogram filtering for geophysical applications," *Geophys. Res. Lett.*, vol. 25, no. 21, pp. 4035–4038, 1998.
63. A. Pepe and R. Lanari, "On the extension of the minimum cost flow algorithm for phase unwrapping of multitemporal differential SAR interferograms," *IEEE Trans. Geosci. Remote Sens.*, vol. 44, no. 9, pp. 2374–2383, Sep. 2006.
64. A. Pepe, L. Euillades, M. Manunta, and R. Lanari, "New advances of the extended minimum cost flow phase unwrapping algorithm for SBASDInSAR analysis at full spatial resolution," *IEEE Trans. Geosci. Remote Sens.*, vol. 49, no. 10, pp. 4062–4079, Oct. 2011.
65. M. Costantini, "A novel phase unwrapping method based on network programming," *IEEE Trans. Geosci. Remote Sens.*, vol. 36, no. 3, pp. 813–821, May 1998.
66. R. Lanari et al., "An overview of the small Baseline subset algorithm: A DInSAR technique for surface deformation analysis," *Pure Appl. Geophys.*, vol. 164, no. 4, pp. 637–661, Jan. 2007, doi: 10.1007/s00024-007-0192-9.

67. M. Manzo, Y. Fialko, F. Casu, A. Pepe, and R. Lanari, "A quantitative assessment of DInSAR measurements of interseismic deformation: The Southern San Andreas fault case study," *Pure Appl. Geophys.*, vol. 169, no. 8, pp. 1463–1482, Aug. 2012.
68. J. Cai, J. Wang, J. Wu, C. Hu, E. Grafarend, J. Chen, "Horizontal deformation rate analysis based on multiepoch GPS measurements in Shanghai," *J. Surv. Eng.* 2008, 134, 132–137.
69. K. Dai, G. Liu, Z. Li, T. Li, B. Yu, X. Wang and A. Singleton, "Extracting Vertical Displacement Rates in Shanghai (China) with Multi-Platform SAR Images," *Remote Sens.* 2015, 7, 9542–9562; doi:10.3390/rs70809542.
70. K. Levenberg, "A Method for the Solution of Certain Non-Linear Problems in Least Squares". *The Quarterly of Applied Mathematics*, 2, pp. 164–168, 1944.
71. D. Marquardt, "An Algorithm for Least-Squares Estimation of Nonlinear Parameters". *SIAM Journal on Applied Mathematics* 11, pp. 431–441, 1963.
72. C. B. Markwardt, "Non-linear Least Squares Fitting in IDL with MPFIT," *Astronomical Data Analysis Software and Systems XVII A.16 ASP Conference Series*, vol. XXX, 2008.
73. Y. Fialko, M. Simons, and D. Agnew, "The complete (3-D) surface displacement field in the epicentral area of the 1999 M(w)7.1 Hector Mine earthquake, California, from space geodetic observations," *Geophys. Res. Lett.*, vol. 28, no. 16, pp. 3063–3066, Aug. 15, 2001.
74. M. Shirzaei, "A seamless multitrack multitemporal InSAR algorithm," *Geosystems. Geochem. Geophys. Geosyst.*, vol. 16, pp. 1656–1669, doi:10.1002/2015GC005759.
75. J. Hu, X. Ding, Z. Li, J. Zhu, Q. Sun, and L. Zhang, "Kalman-Filter-Based Approach for Multisensor, Multitrack, and Multitemporal InSAR," *IEEE Transaction on Geoscience and Remote Sensing*, vol. 51, no. 7, July 2013.
76. M. Manzo, G. P. Ricciardi, F. Casu, G. Ventura, G. Zeni, S. Borgstrom, P. Berardino, C. Del Gaudio, R. Lanari, "Surface deformation analysis in the Ischia Island (Italy) based on spaceborne radar interferometry," *J. Volcanol. Geotherm. Res.*, vol. 151, pp. 399–416, 2006.
77. N. Gourmelen, F. Amelung, F. Casu, M. Manzo, and R. Lanari, "Mining-related ground deformation in Crescent Valley, Nevada: Implications for sparse GPS networks," *Geophys. Res. Lett.*, vol. 34, L09309, doi:10.1029/2007GL029427.
78. S. Samsonov, N. d'Oreye, "Multidimensional time-series analysis of ground deformation from multiple InSAR data sets applied to Virunga Volcanic Province", *Geophysical Journal International*, vol. 191, pp. 1095–1108, 2012.
79. A. Pepe, G. Solaro, F. Calò and C. Dema, "A Minimum-Acceleration Approach for the Retrieval of Multi-Platform InSAR Deformation Time-Series," *IEEE Journal of Selected Topics in Applied Earth Observations and Remote Sensing* (in press), 2016.
80. R. Torres, P. Snoeijs, D. Geudtner, D. Bibby, M. Davidson, E. Attema, P. Potin, B. Rommen, N. Floury, M. Brown, I. Navas Traver, P. Deghaye, B. Duesmann, B. Rosich, N. Miranda, C. Bruno, M. L'Abbate, R. Croci, A. Pietropaolo, M. Huchler, F. Rostan, "GMES Sentinel-1 mission", *Remote Sens. Environ.*, vol. 120, pp. 9–24, May 2012.



© 2016 by the authors; licensee *Preprints*, Basel, Switzerland. This article is an open access article distributed under the terms and conditions of the Creative Commons by Attribution (CC-BY) license (<http://creativecommons.org/licenses/by/4.0/>).